Available online at www.sciencedirect.com

ScienceDirect

IFAC PapersOnLine 55-6 (2022) 760–766

High-Gain Observer-Based Fault Detection Scheme for Short-Circuit Switch Faults in Grid-Connected PV Systems by using Optimizers

Fernando Ivan Mariscal-Castillo * **D. R. Espinoza-Trejo** *
José Ángel Pecina-Sánchez * **Adriana Aguilera-Gonzalez** **
Shamsodin Taheri ***

* *Universidad Autónoma de San Luis Potosí, San Luis Potosí, S.L.P, 78320 Mex (e-mail: mariscal@ieee.org).*
** *University of Bordeaux, ESTIA Institute of Technology, 90 allée Fauste d'Elhuyar, Technopole Izarbel, 64210 Bidart, FR.*
*** *Dept. Computer Science and Engineering,Universite du Québec en Outaouais,Gatineau, Canada.*

Abstract: This paper proposes a model-based fault diagnosis scheme for grid-connected photovoltaic systems with distributed maximum power point tracking (MPPT) strategy. Specifically, short-circuit switch faults in optimizers (boost dc/dc converters in series connection for MPPT purposes) are considered in this study. Depending on the application, SCFs can be more or less detrimental to the stability and integrity of systems. In systems with high penetration, disturbances in voltage or frequency can be generated that can, in the worst case, cause instabilities in the system. Hence, a fast fault detection strategy is mandatory. It is worth noting that, unlike other works reported to date, the control action of the optimizers presents singularities under this fault scenario, making the fault diagnosis task difficult. For this, a decoupled subsystem from i) dc/ac converter dynamics and ii) irradiance changes are obtained for fault and disturbance isolation purposes. Then, a dedicated high-gain observers bank is proposed for a residual generation. In this way, fault time detection is achieved in 8 switching periods. Finally, a numerical evaluation has been carried out to validate the ideas proposed in this paper. For this, three series-connected optimizers interconnected to a three-phase 220V 60 Hz grid through a neutral point clamped (NPC) inverter with a first-order L filter were considered in the simulation.

Keywords: High-Gain Observer, FD algorithm, Optimizers, Distributed Generation, Photovoltaic Converters.

1. INTRODUCTION

In recent years, electricity demand has been increasing. However, it has widely been satisfied by using fossil fuels, which represent a tremendous negative impact on health and the environment. For this reason, collective efforts have been aimed at finding energy sources with a lower carbon footprint. Renewable sources, such as solar photovoltaic or wind, have become very popular in recent years due to their attractive benefits, decreasing costs, and to some extent, their easy installation. Even in 2020, in full contingency due to COVID-19, the photovoltaic solar market achieved a record growth of 18%, with 138 *GW* installed according to Solar Power Europe (2020). However, photovoltaic systems generate an important injection of active power to the main grid, leading to several technical challenges, such as active filtering, voltage and frequency support, operation in island mode, and others.

There are several issues of grid-connected PV systems, such as intermittences in the supply, where generation is only available during specific periods of the day. Other are faults in the switches of the power converters, which serve as an interface between the renewable generation sources and the electrical grid and can cause a degraded generation, or in the worst of cases, instabilities in the system. Several works have been presented in the literature to solve these possible drawbacks of renewable energies. Distributed generation systems have shown a significant reduction in intermittence problems, as long as the sizing of the system is adequate, as shown in Sallam and Malik (2018). Regarding systems based exclusively on photovoltaic energy, the use of serial optimizers has gained significant relevance thanks to its efficiency, improved security, and distributed maximum power point trackers (DMPPT) algorithms, as presented in Espinoza-Trejo et al. (2020).

Fault diagnosis is essential to achieve fault-tolerant control. In the field of FDI, various articles have been presented. In Siouane et al. (2018), an open and short circuit fault-tolerant control scheme is presented in step-up and step-down converters with fixed voltage at the output of

10.1016/j.ifacol.2022.07.218

the step-up stage, using the inductor current in the detection and isolation task. In the work presented by Jamshidpour et al. (2014), open and short circuit fault detection algorithm in boost converters for photovoltaic applications using the switching signal and the inductor current for the FD task is presented. The algorithm can detect a fault in almost two switching cycles in this work. In this paper, it is essential to note that input is a constant voltage source instead of a variable current source that depends on irradiance and temperature, as in PV applications. In the work presented by Espinoza-Trejo et al. (2019), an algorithm based on high-gain observers is presented for boost converters with a photovoltaic module (PVM) as power supply and a battery bank as load, performing the FD scheme in a closed-loop. The authors prove a rapid convergence and insensitivity to power changes from the PVM.

This work presents an FD algorithm operating under the influence of a closed-control action for short-circuit faults in optimizers for grid-connected photovoltaic system configurations. This algorithm is an extesion of the FDI scheme proposed by Espinoza-Trejo et al. (2019) for open- and short-circuit faults in a dc/dc boost converter by using a high-gain observer.. The main contribution of this paper is to demonstrate that a dedicated high-gain observers bank can detect short-circuit faults in m series-connected dc/dc boost converters. In addition, the ac-dynamics is taken into account in this study for FD purposes. Thus, different from previous techniques, batteries are not taken into account in the system design that can considerably enhance the accuracy of fault detection. The nominal system is illustrated in Fig. 1, composed of PVMs with cascade boost optimizers interconnected with a three-phase electrical grid through an NPC inverter with a first-order filter.

The rest of the article is organized as follows. The nominal model of the system is presented in Sec. 2. The nominal control of the system is presented in Sec. 3. In Sec. 4, the fault model and the diagnostic scheme are presented. In Sec. 5, the numerical validation of the proposed algorithm is presented. Finally, the conclusions are presented.

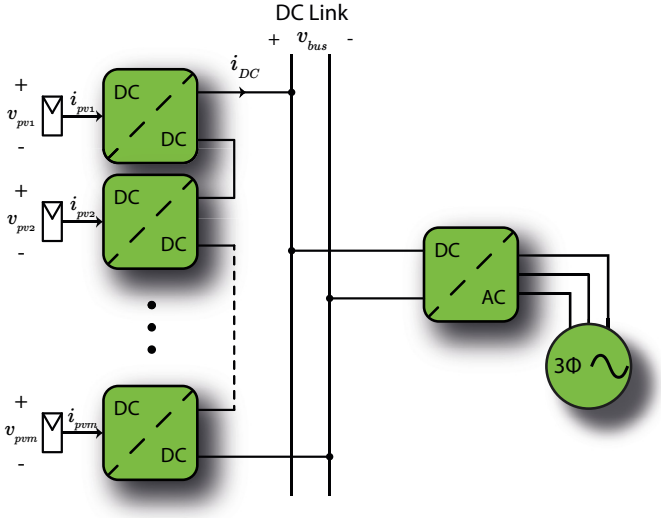

Fig. 1. Nominal System.

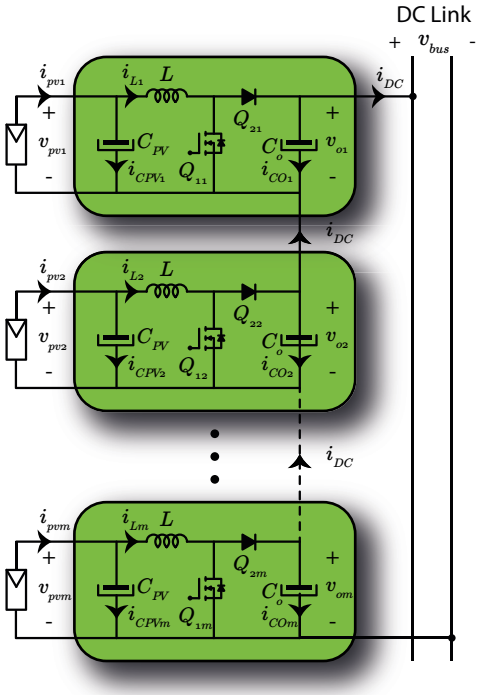

Fig. 2. Optimizers Topology.

2. MATHEMATICAL MODELLING

This section presents the modelling of the nominal system, which is illustrated in Fig. 1. The studied system considers m cascade optimizers interconnected to the electrical grid through a three-phase NPC inverter. Each optimizer is fed by a PV module and connected in a cascade. The whole optimizer bank is connected parallel to the dc-link, thereby providing the power injected by the NPC inverter into the electrical grid. In order to develop a mathematical model of the nominal system, this is split into two parts: parts, i.e., the modelling of the PV optimizers bank and NPC inverter, which are coupled through the bus dc current.

In the following, upright capital letters denote matrices, and bold lower-case letters are used for vectors.

2.1 Optimizer Bank Model

By considering m-series-connected boost dc/dc converters, the mathematical model is derived following a similar approach as in Espinoza-Trejo et al. (2020). The averaged model of the j-th boost dc/dc converter, $\forall j \in \mathfrak{M} = \{1, 2, \ldots, m\}$, is given by three differential equations:

$$C_{PV}\dot{x}_1^j = i_{pv}^j - x_2^j, \tag{1a}$$

$$L\dot{x}_2^j = x_1^j - \left(1 - u^j\right) x_3^j, \tag{1b}$$

$$C_o\dot{x}_3^j = -i_{dc} + \left(1 - u^j\right) x_2^j, \tag{1c}$$

where $x_1^j \triangleq v_{pv}^j$, $x_2^j \triangleq i_L^j$, and $x_3^j \triangleq v_o^j$ represent the voltage of j-th input capacitor C_{pv}, the current of the j-th inductor L and the voltage of the j-th output capacitor C_o, respectively. Thus, the state vector is defined as: $x = [x_1, x_2, x_3]^\top$. The terms i_{pv}^j and i_{dc} in (1) represent the currents flowing through the j-th PV module and the output current, respectively. Also, u^j represents the duty

cycle of the j-th converter. Finally, note that the dc-link voltage can be expressed as:

$$v_{bus} = \sum_{j=1}^{m} x_3^j. \tag{2}$$

2.2 Three-Phase NPC Inverter Model

This section shows a mathematical model for a three-phase NPC inverter interconnected to the electrical grid. In the equivalent circuit, each phase is connected to the grid through a first-order RL filter, where R represents electrical losses and L the inductance in the filter. This model is obtained in the fixed frame $\alpha\beta$ by following a procedure similar as in Escobar et al. (2004). Hence, and by considering Clarke's transform, the averaged inverter model is represented by the following nonlinear differential equations:

$$L\dot{\boldsymbol{x}}_{\alpha\beta} = -R\boldsymbol{x}_{\alpha\beta} + \boldsymbol{e}_{\alpha\beta} - \boldsymbol{v}_{\alpha\beta} \tag{3}$$

$$C\dot{x}_{bus} = 2i_{dc} - \boldsymbol{u}_{\alpha\beta}^{\top}\boldsymbol{x}_{\alpha\beta} \tag{4}$$

$$C\dot{x}_{bal} = -\sqrt{\frac{2}{3}}\left[\frac{1}{2}\left(u_\alpha^2 - u_\beta^2\right),\ -u_\alpha u_\beta\right]\boldsymbol{x}_{\alpha\beta} - \frac{2}{\sqrt{3}}\boldsymbol{u}_{\alpha\beta}^{\top}\boldsymbol{x}_{\alpha\beta}d_0, \tag{5}$$

where $\boldsymbol{x}_{\alpha\beta} \triangleq [i_\alpha\ \ i_\beta]^{\top}$ represents $\alpha\beta$ currents components, $\boldsymbol{e}_{\alpha\beta} \triangleq [u_\alpha\ \ u_\beta]^{\top}$ is the output voltage of the inverter in the fixed frame $\alpha\beta$, $\boldsymbol{v}_{\alpha\beta} \triangleq [v_\alpha\ \ v_\beta]^{\top}$ represents the $\alpha\beta$ components of electrical grid voltage, $\boldsymbol{u}_{\alpha\beta 0} \triangleq [u_\alpha\ \ u_\beta\ \ u_0]^{\top}$ is the averaged control signal in the fixed frame $\alpha\beta$, $x_{bus} \triangleq v_{c1} + v_{c2}$ denotes the sum of the voltage at the capacitors and x_{bal} its difference, i.e., $x_{bal} \triangleq v_{c1} - v_{c2}$. It is worth noting that both the dynamics of the optimizers and inverter depend on the arbitrary and unknown variable i_{dc}, so detection on the dc side can be affected by phenomena on the ac side.

2.3 Nominal System Model

The model that includes the dynamics of m-cascade optimizers and a three-phase NPC inverter connected to the electrical grid is given in the following.

Considering (1c), (2) and (4), i_{dc} can be written as:

$$i_{dc} = \Lambda\left[\frac{C}{C_o}\sum_{j=1}^{m}\left(1-u^j\right)x_2^j + \boldsymbol{u}_{\alpha\beta}^{\top}\boldsymbol{x}_{\alpha\beta}\right], \tag{6}$$

where $\Lambda = C_o/\left(2C_o + mC\right)$. Substituting (6) into (1c) and (4), the next nonlinear differential equations are obtained:

$$C_o\dot{x}_3^j = -\Lambda\left[\frac{C}{C_o}\sum_{\ell=1}^{m}\left(1-u^\ell\right)x_2^\ell + \boldsymbol{u}_{\alpha\beta}^{\top}\boldsymbol{x}_{\alpha\beta}\right] + \cdots \cdots + \left(1-u^j\right)x_2^j \tag{7}$$

$$C\dot{x}_{bus} = 2\Lambda\left[\frac{C}{C_o}\sum_{\ell=1}^{m}\left(1-u^\ell\right)x_2^\ell + u_{\alpha\beta}^{\top}x_{\alpha\beta}\right] - \cdots \cdots - u_{\alpha\beta}^{\top}\boldsymbol{x}_{\alpha\beta} \tag{8}$$

Thus, the mathematical model for the nominal system can be written compactly as:

$$\dot{\boldsymbol{x}} = \boldsymbol{A}\boldsymbol{x} + \sum_{j=1}^{m}\boldsymbol{g}_1^j(\boldsymbol{x})\,u^j + \sum_{\ell\in\{\alpha,\beta\}}\boldsymbol{g}_2^\ell(\boldsymbol{x})\,u_\ell + \cdots \cdots + \boldsymbol{D}\boldsymbol{i}_{\boldsymbol{pv}} + \boldsymbol{v}_{\alpha\beta}, \tag{9}$$

$$\dot{x}_{bal} = f\left(x_{\alpha\beta}, u_{\alpha\beta 0}\right), \tag{10}$$

$$y = \boldsymbol{C}\boldsymbol{x} = \boldsymbol{I}_{3m+3}\boldsymbol{x}, \tag{11}$$

where the state vector is defined by:

$$\boldsymbol{x} = \left(\boldsymbol{x}^1, \boldsymbol{x}^2, \ldots, \boldsymbol{x}^m, x_\alpha, x_\beta, x_{bus}\right).$$

Hence, $\boldsymbol{x} \in \mathbb{R}^{3m+3}$ and $\boldsymbol{x}^j \in \mathbb{R}^3\ \forall\ j \in \mathfrak{M} = \{1, 2, \ldots, m\}$ is given by:

$$\boldsymbol{x}^j = \left(x_1^j, x_2^j, x_3^j\right).$$

The matrix $\boldsymbol{I}_{3m+3}$ denotes the matrix of order $3m+3$. Also, the matrix $\boldsymbol{A} \in \mathbb{R}^{(3m+3)\times(3m+3)}$ is defined as:

$$\boldsymbol{A} = \begin{bmatrix} \boldsymbol{A}^1 & \boldsymbol{k}_0 & \cdots & \boldsymbol{k}_0 & \boldsymbol{0} & \boldsymbol{0} & \boldsymbol{0} \\ \boldsymbol{k}_0 & \boldsymbol{A}^2 & \cdots & \boldsymbol{k}_0 & \boldsymbol{0} & \boldsymbol{0} & \boldsymbol{0} \\ \vdots & \vdots & \ddots & \vdots & \vdots & \vdots & \vdots \\ \boldsymbol{k}_0 & \boldsymbol{k}_0 & \cdots & \boldsymbol{A}^m & \boldsymbol{0} & \boldsymbol{0} & \boldsymbol{0} \\ \boldsymbol{0} & \boldsymbol{0} & \cdots & \boldsymbol{0} & -RL^{-1} & 0 & 0 \\ \boldsymbol{0} & \boldsymbol{0} & \cdots & \boldsymbol{0} & 0 & -RL^{-1} & 0 \\ \boldsymbol{k}_1 & \boldsymbol{k}_1 & \cdots & \boldsymbol{k}_1 & 0 & 0 & 0 \end{bmatrix}, \tag{12}$$

where $\boldsymbol{0}$ is a null matrix or vector of appropriate dimensions, and the matrices $\boldsymbol{A}^j, \boldsymbol{k}_0, \in \mathbb{R}^{3\times 3}$ and the vector $\boldsymbol{k}_1 \in \mathbb{R}^3$ are defined by:

$$\boldsymbol{A}^j = \begin{bmatrix} 0 & -\frac{1}{C_{pv}} & 0 \\ \frac{1}{L} & 0 & -\frac{1}{L} \\ 0 & 1-\frac{\Lambda C}{C_o} & 0 \end{bmatrix}\ \forall j \in \mathfrak{M} = \{1, 2, \ldots, m\}, \tag{13}$$

$$\boldsymbol{k}_0 = \begin{bmatrix} 0 & 0 & 0 \\ 0 & 0 & 0 \\ 0 & -\frac{\Lambda C}{C_o} & 0 \end{bmatrix}, \tag{14}$$

$$\boldsymbol{k}_1 = \begin{bmatrix} 0 & 2\frac{\Lambda C}{C_o} & 0 \end{bmatrix}. \tag{15}$$

The vector fields $\boldsymbol{g}_1^j(\boldsymbol{x}) \in \mathbb{R}^{3m+3}$ are represented by:

$$\boldsymbol{g}_1^1(\boldsymbol{x}) = \left[\boldsymbol{g}_1\left(\boldsymbol{x}^1\right), \boldsymbol{h}\left(\boldsymbol{x}^1\right), \ldots, \boldsymbol{h}\left(\boldsymbol{x}^1\right), \boldsymbol{i}\left(\boldsymbol{x}^1\right)\right]^{\top},$$
$$\boldsymbol{g}_1^2(\boldsymbol{x}) = \left[\boldsymbol{h}\left(\boldsymbol{x}^2\right), \boldsymbol{g}_1\left(\boldsymbol{x}^2\right), \ldots, \boldsymbol{h}\left(\boldsymbol{x}^2\right), \boldsymbol{i}\left(\boldsymbol{x}^2\right)\right]^{\top},$$
$$\vdots$$
$$\boldsymbol{g}_1^m(\boldsymbol{x}) = \left[\boldsymbol{h}\left(\boldsymbol{x}^m\right), \ldots, \boldsymbol{h}\left(\boldsymbol{x}^m\right), \boldsymbol{g}_1\left(\boldsymbol{x}^m\right), \boldsymbol{i}\left(\boldsymbol{x}^m\right)\right]^{\top},$$

where

$$\boldsymbol{g}_1\left(\boldsymbol{x}^j\right) = \left[0, L^{-1}x_3^j, \left(\Lambda C C_o^{-2} - C_o^{-1}\right)x_2^j\right]^{\top}, \tag{16}$$

$$\boldsymbol{h}\left(\boldsymbol{x}^j\right) = \left[0, 0, \Lambda C C_o^{-2}x_2^j\right]^{\top}, \tag{17}$$

$$\boldsymbol{i}\left(\boldsymbol{x}^j\right) = \left[0, 0, -2\Lambda C_o^{-1}x_2^j\right]^{\top}. \tag{18}$$

The control inputs u^j denote the duty cycle for each switch Q_{1j}, as shown in Fig. 2. While the vector fields $\boldsymbol{g}_2^\ell(\boldsymbol{x}) \in \mathbb{R}^{3m+3}$ are defined by:

$$\boldsymbol{g}_2^\alpha(\boldsymbol{x}) = \left[\boldsymbol{g}_2\left(\boldsymbol{x}_\alpha\right), \ldots, \boldsymbol{g}_2\left(\boldsymbol{x}_\alpha\right), 1/2x_{bus}, 0, \left(2\Lambda - 1\right)x_\alpha\right]^{\top},$$
$$\boldsymbol{g}_2^\beta(\boldsymbol{x}) = \left[\boldsymbol{g}_2\left(\boldsymbol{x}_\beta\right), \ldots, \boldsymbol{g}_2\left(\boldsymbol{x}_\beta\right), 0, 1/2x_{bus}, \left(2\Lambda - 1\right)x_\beta\right]^{\top},$$

where $\boldsymbol{g}_2(\boldsymbol{x}_\ell) = [0, 0, -\Lambda x_\ell]^\top$. The control inputs d_ℓ denote the inverter control signals in the fixed frame $\alpha\beta$. Matrix $\boldsymbol{D} \in \mathbb{R}^{(3m+3)\times(m+3)}$ is given by:

$$\boldsymbol{D} = \begin{bmatrix} \boldsymbol{d}_1 & \boldsymbol{0}^\intercal & \dots & \boldsymbol{0}^\intercal & 0 & 0 & 0 \\ \boldsymbol{0}^\intercal & \boldsymbol{d}_2 & \dots & \boldsymbol{0}^\intercal & 0 & 0 & 0 \\ \boldsymbol{0}^\intercal & \boldsymbol{0}^\intercal & \dots & \boldsymbol{0}^\intercal & 0 & 0 & 0 \\ \boldsymbol{0}^\intercal & \boldsymbol{0}^\intercal & \dots & \boldsymbol{d}_m & 0 & 0 & 0 \\ 0 & 0 & \cdots & 0 & 0 & 0 & 0 \\ 0 & 0 & \cdots & 0 & 0 & 0 & 0 \\ 0 & 0 & \cdots & 0 & 0 & 0 & 0 \end{bmatrix},$$

where $\boldsymbol{d}_j \in \mathbb{R}^3$ is defined as $\boldsymbol{d}_j = \left[C_{pv}^{-1}, 0, 0\right]^\intercal$, and $\boldsymbol{i}_{pv}$ denotes the vector of PV currents as:

$$\boldsymbol{i}_{pv} = [i_{pv1}, i_{pv2}, \dots, i_{pvm}, 0, 0, 0].$$

Vector $\boldsymbol{v}_{\alpha\beta} \in \mathbb{R}^{3m+3}$ is defined by:

$$\boldsymbol{v}_{\alpha\beta} = \left[0, 0, \cdots, 0, -L^{-1}v_\alpha, -L^{-1}v_\beta, 0\right]^\top. \tag{19}$$

Finally, function f in (10) is given by:

$$f(x_{\alpha\beta}, u_{\alpha\beta 0}) = -\sqrt{\frac{2}{3}}\left[\frac{1}{2}\left(u_\alpha^2 - u_\beta^2\right), \ -u_\alpha u_\beta\right] x_{\alpha\beta} \cdots \\ \cdots - \frac{2}{\sqrt{3}} u_{\alpha\beta}^\top x_{\alpha\beta} d_0. \tag{20}$$

Departing from this model, the nominal control and the fault detection schemes will be developed in the following sections.

3. NOMINAL CLOSED-LOOP CONTROL

In this section, nominal control is designed by considering active power injection as the primary control objective of the nominal system. Therefore, the inverter's nominal control must achieve the following tasks: dc-link regulation, dc-link balance, and power factor unitary. These tasks can be fulfilled by dividing the control law into an inner-control loop (current loop) and an outer loop (voltage loop). The control strategy adopted for both control loops corresponds to a proportional-resonant (PR) control and PI control, respectively. The structure of the control loops, as well as their tuning, for the inverter subsystem, can be consulted in detail in Escobar et al. (2004).

The control actions that ensure maximum power extraction from PVMs. is accomplished, corresponds to the control law for the PV optimizers proposed by Espinoza-Trejo et al. (2020), which is presented as follow:

$$u^j = \left(\frac{x_3^j - x_1^j}{x_3^j}\right) - \frac{1}{x_3^j}\nu^j, \tag{21}$$

$$\nu^j = k_p \tilde{x}_1^j + k_i \int \tilde{x}_1^j dt + k_d C_{pv}^{-1}\left(x_2^j - i_{pv}^j\right), \tag{22}$$

where $\tilde{x}_1^j \triangleq x_1^{j,*} - x_1^j$ represents the error between the PV voltage x_1^j and the voltage reference (MPP voltage) $x_1^{j,*}$. Here, the setpoint is assumed to be piece-wise constant or slowly time varying. It is worth noting in (21) that voltage x_3^j is measurable, which is crucial for developing the FD algorithm presented in the next section of this paper.

It is possible to use the optimizer's nominal controller presented in (21) and (22) for the fault detection task. Using this signal and with a priori knowledge of the system model, it is possible to build a high-gain observer. The main task of this observer will be the estimation of the states for residual generation. The following sections show the impact of this on detecting SCF.

4. FAULT DIAGNOSIS SCHEME

4.1 Fault Modeling

In order to show the impact of a short-circuit fault on the system, in this section, the model of this kind of fault is presented. For this purpose, an additive structure is proposed for short-circuit faults (SCF) in the actuator, i.e.,

$$u^j = u_o^j + \delta_f^j. \tag{23}$$

For simplicity, analysis can be done under steady-state conditions. As consequence, (23), is expressed as:

$$U^j = U_o^j + \Delta_f^j, \tag{24}$$

where u^j and U^j represent the temporary control signal and under steady-state conditions, u_o^j and U_o^j symbolize the temporary nominal control and under steady-state, finally, δ_f^j and Δ_f^j represents fault the temporary and steady-state contribution of the fault to control signal.

In the absence of faults, i.e. $\forall t < t_f$, where t_f is the fault triggering time. The following conditions are reached by the nominal control action in steady-state:

$$\lim_{t\to\infty} x_1^j = x_1^{j,*} = X_1^j, \tag{25}$$

$$\lim_{t\to\infty} x_2^j = i_{pv}^j = X_2^j, \tag{26}$$

$$\lim_{t\to\infty} x_3^j = X_3^j, \tag{27}$$

where X_1^j, X_2^j and X_3^j represent the steady state of the state variables x_1^j, x_2^j and x_3^j, respectivley. As a consequence, ν in (21) go down to zero at steady state condition and the nominal control will be given by:

$$U_o^j = 1 - \frac{X_1^{j,*}}{X_3^j}. \tag{28}$$

By considering the addition of the fault effect to the steady-state control signal, control function U^j is given by:

$$U^j = \underbrace{\left(1 - \frac{X_1^{j,*}}{X_3^j}\right)}_{U_o^j} + \underbrace{\frac{X_1^{j,*} - X_1^j}{X_3^j} - \frac{1}{X_3^j}\mathcal{N}}_{\Delta_f^j}, \tag{29}$$

where $\mathcal{N}$ stands for ν^j in steady-state. Note that in the absence of fault, Δ_f^j contribution to control signal is zero. In the presence of a SCF, i.e. $\forall t > t_f$. The following steady-state conditions are obtained:

$$\lim_{t\to\infty} x_1^j = X_1^j = 0, \tag{30}$$

$$\lim_{t\to\infty} x_2^j = i_{pv}^j = X_2^j = I_{sc}^j, \tag{31}$$

$$\lim_{t\to\infty} x_3^j = X_3^j = 0. \tag{32}$$

Under these conditions, $\mathcal{N}$ is expressed as follows:

$$\mathcal{N} = X_1^{j,*}(k_p + k_i t) \tag{33}$$

and control (29) becomes:

$$U^j = \left(1 - \frac{X_1^{j,*}}{X_3^j}\right) - \frac{X_1^{j,*}\left[(k_p - 1) + k_i t\right]}{X_3^j}. \tag{34}$$

Observe that (34) presents a singularity in the terms of the right hand. Consequently, it is impossible to model U^j under short-circuit faults, and its numerical convergence will depend 100% on the platform on which the control algorithm is executed. Without a fault modelling that describes the behaviour of the control signal, the use of the control signal without considering the dynamics of the optimizer for FDI purposes is not feasible.

However, considering the evaluation of (34) in (1b) (optimizer's current dynamics) for FDI purposes, the following expression is obtained:

$$L\dot{X}_2^j = -X_1^{j,*}\left(k_p + k_i t\right). \tag{35}$$

Note that there is not a singularity in this expression due to the product of the control function U^j and X_3^j. As control gains are positive constants, i.e., $k_p > 0$ and $k_i > 0$, then $\dot{x}_2^j < 0$ for $t > t_f$ and $\dot{x}_2^j \notin \ell_\infty$. This fault profile can be exploited for fault detection purposes, which will be used in the next section.

Remark. It is worth nothing that (35) represents how the control law tries to avoid the SCF by decreasing the PV current, and should not be confused with the real dynamics of the current.

4.2 Fault Diagnosis Scheme

This section shows the generalization of the FD algorithm based on a bank of high-gain observers, designed as described in Espinoza-Trejo et al. (2019) for m cascaded boost converters interconnected to the electrical grid. A decoupled subsystem from dc/ac converter dynamics and irradiance changes can be obtained from the model given in (9). For this, the output voltage $y_2^j = x_3^j$ (for each optimizer), which is a common measure for MPPT algorithms, is considered an available measurement of the system. This subsystem is given as:

$$\dot{\boldsymbol{x}}_{d1} = \mathbf{A}_{d1}\boldsymbol{x}_{d1} + \boldsymbol{G}\left(u^j, i_{pv}^j, y_2^j\right) + \boldsymbol{F}\tilde{\delta}_f \;\forall j, \tag{36}$$

$$\dot{\boldsymbol{x}}_{d2} = \mathbf{A}_{d2}\boldsymbol{x}_{d2} + \boldsymbol{H}\left(u_{\alpha\beta}, y_2^j\right) + \boldsymbol{v}_{\alpha\beta} \;\forall j, \tag{37}$$

$$\boldsymbol{y}_1 = \boldsymbol{C}_d\boldsymbol{x}_d = \left[\boldsymbol{C}_d^1, \boldsymbol{C}_d^2 \cdots \boldsymbol{C}_d^m\right]^\top \boldsymbol{x}_d, \tag{38}$$

where $\dot{\boldsymbol{x}}_{d1}$ and $\dot{\boldsymbol{x}}_{d2}$ groups the optimizer's and the inverter's dynamics respectively as two decoupled systems. The new state vectors are defined by:

$$\boldsymbol{x}_{d1} = \left(\boldsymbol{x}_d^1, \boldsymbol{x}_d^2, \ldots, \boldsymbol{x}_d^m\right)^\top,$$
$$\boldsymbol{x}_{d2} = \left(x_\alpha, x_\beta\right)^\top,$$

where $\boldsymbol{x}_{d1} \in \mathbb{R}^{2m}$, $\boldsymbol{x}_{d2} \in \mathbb{R}^2$ and $\boldsymbol{x}_d^j \in \mathbb{R}^2 \;\forall\; j \in \mathfrak{M} = \{1, 2, \ldots, m\}$ is given by:

$$\boldsymbol{x}_d^j = \left(x_1^j, x_2^j\right)^\top.$$

The output jth output matrix is defined as $\boldsymbol{C}_d^j = [1, 0]$. The fault input $\tilde{\delta}_f^j = y_2^j\delta_f^j$ with $y_2^j \geq 0 \forall t$. The matrices $\boldsymbol{A}_{d1} \in \mathbb{R}^{(2m)\times(2m)}$ and $\boldsymbol{A}_{d2} \in \mathbb{R}^{2\times 2}$ are defined as:

$$\boldsymbol{A}_{d1} = \begin{bmatrix} \boldsymbol{A}_d^1 & \mathbf{0} & \cdots & \mathbf{0} \\ \mathbf{0} & \boldsymbol{A}_d^2 & \cdots & \mathbf{0} \\ \vdots & \vdots & \ddots & \vdots \\ \mathbf{0} & \mathbf{0} & \cdots & \boldsymbol{A}_d^m \end{bmatrix}, \tag{39}$$

$$\boldsymbol{A}_{d2} = \begin{bmatrix} -RL^{-1} & 0 \\ 0 & -RL^{-1} \end{bmatrix}, \tag{40}$$

where $\mathbf{0} \in \mathbb{R}^2$ is a null matrix, and $\boldsymbol{A}_d^j \in \mathbb{R}^{2\times 2}$ is defined by:

$$\boldsymbol{A}_d^j = \begin{bmatrix} 0 & -C_{pv}^{-1} \\ L^{-1} & 0 \end{bmatrix} \;\forall j \in \mathfrak{M} = \{1, 2, \ldots, m\}, \tag{41}$$

the vectors field $\boldsymbol{G} \in \mathbb{R}^{2m}$ and $\boldsymbol{H} \in \mathbb{R}^2$ are represented by:

$$\boldsymbol{G} = \begin{bmatrix} \boldsymbol{g}_d(u^1, i_{pv}^1, y_2^1) \\ \boldsymbol{g}_d(u^2, i_{pv}^2, y_2^2) \\ \vdots \\ \boldsymbol{g}_d(u^m, i_{pv}^m, y_2^m) \end{bmatrix}, \tag{42}$$

$$\boldsymbol{H} = \begin{bmatrix} \boldsymbol{h}_d(u_\alpha, y_2^1, \ldots, y_2^m) \\ \boldsymbol{h}_d(u_\beta, y_2^1, \ldots, y_2^m) \end{bmatrix}, \tag{43}$$

where $\boldsymbol{g}_d(u^j, i_{pv}^j, y_2^j)$ and $\boldsymbol{h}_d(u_\ell, y_2^1, \ldots, y_2^m)$ are defined as:

$$\boldsymbol{g}_d(u^j, i_{pv}^j, y_2^j) = \left[i_{pv}^j, -L^{-1}y_2^j(1 - u^j)\right]^\top \tag{44}$$

$$\boldsymbol{h}_d(u_\ell, y_2^1, \ldots, y_2^m) = (2L)^{-1}\sum_j y_2^j u_\ell \tag{45}$$

$$\forall j \quad \in \{1, 2, \ldots, m\},$$
$$\forall \ell \quad \in \{\alpha, \beta\},$$

it is worth noting that the second term of the vector field $\boldsymbol{g}_d(u^j, i_{pv}^j, y_2^j)$ presents the dynamics expressed in (35) under SCF. Thus, its use is foreseen within the observer presented in the following subsection. The vector $\boldsymbol{v}_{\alpha\beta,d} \in \mathbb{R}^2$ is defined by:

$$\boldsymbol{v}_{\alpha\beta} = \left[-L^{-1}v_\alpha, -L^{-1}v_\beta\right]^\top. \tag{46}$$

Finally, the vector $\boldsymbol{F} \in \mathbb{R}^{2m}$ is defined as:

$$\boldsymbol{F} = [\boldsymbol{f}_d, \boldsymbol{f}_d, \ldots, \boldsymbol{f}_d], \tag{47}$$

where $\boldsymbol{f}_d = \left[0, L^{-1}\right]^\top$.

4.3 Residual Generator

This work proposes a high-gain bank observer for short-circuit fault detection in boost dc/dc converters in series connection. Using a high-gain observer ensures fast convergence, robustness against parametric uncertainties or model inaccuracy. As a consequence of the decoupled system, a dedicated observer scheme (DOS) is proposed for the system, where an HGO is dedicated to states estimation in each dc/dc converter.

$$\dot{z}^j = \boldsymbol{A}_o^j\boldsymbol{z}^j + \mathcal{O}\boldsymbol{G}\left(u^j, \boldsymbol{i}_{pv}^j, y_2^j\right) + \mathcal{O}\boldsymbol{F}^j\tilde{\delta}_f^j \tag{48}$$

$$\boldsymbol{y}_1^j = \boldsymbol{C}_o\boldsymbol{z}^j, \tag{49}$$

where $\mathcal{O} \in \mathbb{R}^{2\times 2}$ is the Kalman observability matrix, $\boldsymbol{z}^j = \left[z_1^j \;\; z_2^j\right] = \mathcal{O}\boldsymbol{x}_d^j$, and

$$\boldsymbol{A}_o^j = \begin{bmatrix} 0 & 1 \\ 0 & 0 \end{bmatrix},$$
$$\boldsymbol{C}_o = [1\ 0].$$

The HGO is designed by neglecting any perturbation and fault condition. The observer structure is given by:

$$\dot{\hat{z}}^j = \boldsymbol{A}_o^j \hat{\boldsymbol{z}}^j + \mathcal{O}\boldsymbol{G}\left(u^j, \boldsymbol{i}_{pv}^j, y_2^j\right) + \cdots$$
$$\cdots + \boldsymbol{\Lambda}_K \boldsymbol{H}_o \left(y_1^j - \boldsymbol{C}_o \hat{z}^j\right), \quad (50)$$
$$y_1^j = \boldsymbol{C}_o \hat{\boldsymbol{z}}^j, \quad (51)$$

whit $K > 0$ and

$$\boldsymbol{\Lambda}_K = \begin{bmatrix} K & 0 \\ 0 & K^2 \end{bmatrix}, \quad (52)$$
$$\boldsymbol{H}_o = \begin{bmatrix} h_1 \\ h_2 \end{bmatrix}. \quad (53)$$

The estimation error dynamic is given by:

$$\dot{e}^j = (\boldsymbol{A}_o^j - \boldsymbol{\Lambda}_K \boldsymbol{H}_o \boldsymbol{C}_o) e^j - \mathcal{O}\boldsymbol{F}^j \quad (54)$$
$$r^j = \boldsymbol{C}_o e^j, \quad (55)$$

where r^j stands for the residual signal. Therefore, the FD condition in the jth optimizer is accomplished with the following decision rule:

$$\text{Decision} = \begin{cases} \text{Fault if} & r^j(t) > J_{TH}, \\ \text{No fault if} & r^j(t) \leq J_{TH}, \end{cases} \quad (56)$$

where J_{TH} is a threshold chosen considering the measurement noise.

5. SIMULATION RESULTS

In order to evaluate the proposed model-based FD technique, the following faulty scenario was computed on Simulink. From $0.0s \leq t < 0.3s$ the system is operated under nominal conditions, $t = 0.3$ s a sudden change in the irradiance occurs from 1.0 kW/m^2 to 0.6 kW/m^2. Finally, an SCF condition is triggered at $t = 0.6$ s. Results were obtained by considering 3 PVMs, each 455 W with its respective optimizer. The parameters of each PVM are listed in Table 1, where V_{MPP} and I_{MPP} stand for voltage and current at the maximum power point in standard test conditions (STC), V_{OC} and I_{SC} are the open-circuit voltage and short-circuit current under STC. The parameters of the boost dc/dc converters are $L_{pv} = 1.0$ mH, $C_{pv} = 600$ μF, $C_o = 10$ μF, and switching frequency of 25 kHz. The control parameters are $k_p = 5.277 \times 10^8$, $k_i = 1.385 \times 10^{12}$ and $k_d = 6.0 \times 10^4$. The parameters of the three-phase NPC inverter are $C = 2000$ μF, $L = 3mH$, and switching frequency of $25kHz$. The control parameters are $k_{inv} = 100$, $\rho_1 = 800$, $k_{p,1} = 5 \times 10^{-3}$, $k_{i,1} = 3.0 \times 1^{-1}$, $k_{p,2} = 20$, $k_{i,2} = 10$. The inverter is connected to a three-phase electrical grid, with line-to-line voltage of $220V$ at $60Hz$. The dc-link voltage is regulated at $600V$. The HGO's parameters are $K = 100$, $h_1 = 8.00 \times 10^3$, $h_2 = 1.60 \times 10^7$, and the threshold jth was selected by inspection with a value of 0.04. The tuning of the bank of observers was elaborated through the pole placement technique with a frequency $\omega_n = 4000.00$ and a damping factor $\xi = 1$.

Table 1. PVMs' Parameters

Parameter	Value	Parameter	Value
V_{MPP}	$41.51V$	I_{MPP}	$10.96A$
V_{OC}	$49.35V$	I_{SC}	$11.44A$

5.1 Short-Circuit Fault

This section shows the experiment carried out under an SCF. Results are presented in Fig. 3. At $t = 0.3s$ a sudden irradiance change occurs, from $1kW/m^2$ to $0.6kW/m^2$. Fig. 3a) to 3c), 3e) to 3g) and 3i) to 3k) shows the transient response of every optimizer's state variables, where only variables x_2^j are affected by the irradiance change. At $t = 0.6s$, an SCF occurs, driving x_1^1 and x_3^1 to zero and x_2^1 to I_{sc}. Consequently, PVM operates at a null efficiency, i.e., PVM has a $0W$ production, which forces the controller for trying to compensate for this failure effect. Due to integral action, control effort leads the observer to diverge. The remaining optimizers continue operating at maximum power point by adjusting their duty cycle, and hence, their output voltage x_3^2 and x_3^3. Fig. 3d) and 3h), respectively, show the dc-link voltage behaviour and the harvesting and injecting power. At $t = 0.0$ s it is observed the transient state due to system start-up, dc-link voltage is regulated to 800 V and, dc and ac power is $1,228$ W. At $t = 0.3s$, dc-link voltage and power show a transient state during irradiance change. Conversely, the inverter control loop regulates the dc-voltage, driving it to $800v$ again. On the other hand, power falls from 1200 W to 735 W. At $t = 0.6s$, PVM1's converter is subjected to an SCF, causing a new transient state in the dc-link voltage and a fall in power from 735 W to 492 W. Residual signal r_1 and fault detection alarm FD are shown in Fig. 3l) and 3p). It should be noted that despite the abrupt change in irradiance at $t = 0.3$ s, the FD algorithm is insensitive to it. At $t = 0.6$ s, the alarm is triggered when the residual begins to increase. Fig. 4 shows the residual r_1 and the fault alarm signal from top to bottom. Also shown is a magnification for better observation of the fault event in the range of 0.599696 s to 0.600304 s. Note that the residual exceeds the 0.04 threshold after 0.000304 s (7.6 switching cycles) after the fault occurred. Control signals of each optimizer and its average are shown in Fig. 3m) to 3o). Note that for the first $0.6s$, the three duty cycles are very similar, although they are close to their physical limit. At $t = 0.6$ s, the first average duty cycle goes to 1 due to SCF, while the remaining optimizers work in a prohibited duty cycle, which indicates the need for accommodation in the presence of this type of faults.

6. CONCLUSION

Optimizers in grid-connected PV applications turn out to be attractive due to their capabilities in power handling, scaling the PVM voltage, or locating different MPPs. This type of system can present singularities in control during a failure event due to the voltage loss at the output of one or more optimizers. This makes the task of detection difficult. This document presented a robust FD algorithm for PV optimizers under SCF interconnected to the electrical grid. The main contribution of this work lies in the correct detection of SCF even under singularities of the optimizer drivers. The proposed FD system is

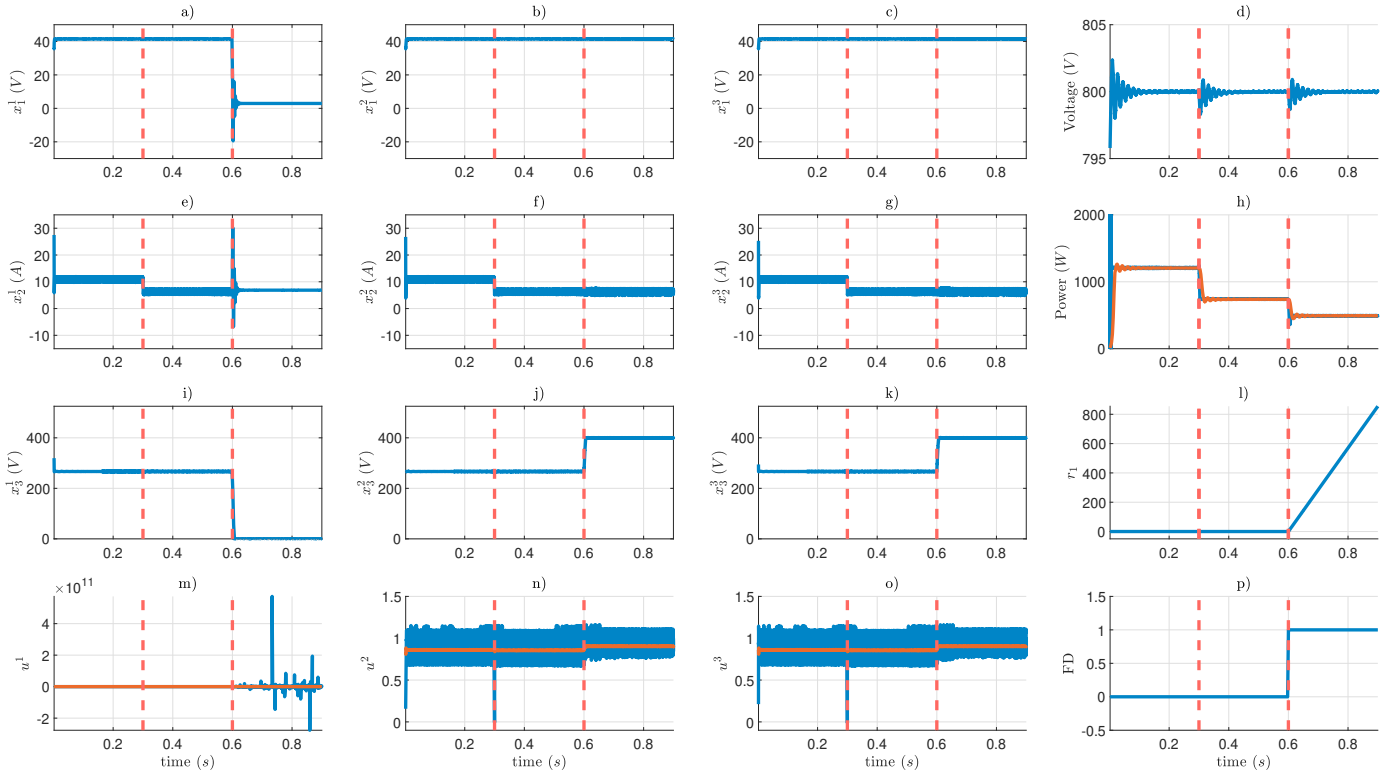

Fig. 3. Simulation results. From top to bottom and from left to right: a)-c) PV voltage x_1^j, d) dc-link voltage, e)-g)inductor current x_2^j, h) power harvested by optimizers (blue) and injected into the electrical grid by the inverter (red), i)-k) the output voltage x_3^j, l) residual signal, m)-o) optimizer's control signals (blue) and their average (red), and p) fault detection alarm.

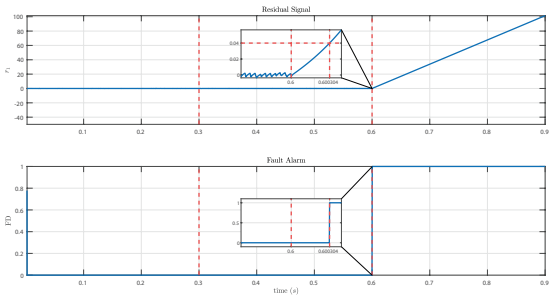

Fig. 4. From top to bottom: residual signal, fault detection alarm.

capable of 1) decoupling the inverter dynamics from the optimizers, 2) detecting short circuit faults even when the optimizer output voltage drops to zero, 3) being insensitive to changes in the power generated by the PVMs .

REFERENCES

Escobar, G., Leyva-Ramos, J., Carrasco, J., Galvan, E., Portillo, R., Prats, M., and Franquelo, L. (2004). Modeling of a three level converter used in a synchronous rectifier application. In 2004 IEEE 35th Annual Power Electronics Specialists Conference (IEEE Cat. No. 04CH37551), volume 6, 4306–4311. IEEE.

Espinoza-Trejo, D.R., Taheri, S., and Pecina-Sánchez, J.A. (2019). Switch fault diagnosis for boost dc–dc converters in photovoltaic mppt systems by using high-gain observers. IET Power Electronics, 12(11), 2793–2801.

Espinoza-Trejo, D.R., Taheri, S., Saavedra, J.L., Vázquez, P., De Angelo, C.H., and Pecina-Sánchez, J.A. (2020). Nonlinear control and internal stability analysis of series-connected boost dc/dc converters in pv systems with distributed mppt. IEEE Journal of Photovoltaics, 11(2), 504–512.

Jamshidpour, E., Poure, P., Gholipour, E., and Saadate, S. (2014). Single-switch dc–dc converter with fault-tolerant capability under open-and short-circuit switch failures. IEEE transactions on power electronics, 30(5), 2703–2712.

Sallam, A.A. and Malik, O.P. (2018). Electric distribution systems. John Wiley & Sons.

Siouane, S., Jovanović, S., Poure, P., and Jamshidpour, E. (2018). An efficient fault tolerant cascaded step-up step-down converter for solar pv modules. In 2018 IEEE International Conference on Environment and Electrical Engineering and 2018 IEEE Industrial and Commercial Power Systems Europe (EEEIC/I&CPS Europe), 1–5. IEEE.

Solar Power Europe (2020). Global market outlook for solar power/2020–2024. Solar Power Europe: Brussels, Belgium.